RSC Advances

This article can be cited before page numbers have been issued, to do this please use: Y. Zhang, J. Wang, G. Han, F. Lu and Q. Tong, *RSC Adv.*, 2016, DOI: 10.1039/C6RA13605B.

ROYAL SOCIETY OF CHEMISTRY

www.rsc.org/advances

View Article Online
DOI: 10.1039/C6RA13605B

Journal Name

ARTICLE

Phenanthroimidazole derivatives as emitters for non-doped deep-blue organic light emitting devices

Received 00th January 20xx,
Accepted 00th January 20xx

DOI: 10.1039/x0xx00000x

www.rsc.org/

Ying Zhang,[a,b] Jun-Hao Wang,[a] Gaoyi Han,[a] Feng Lu*[b] and Qing-Xiao Tong*[b]

A series of phenanthroimidazole derivatives with N-1 and C-2 position modification have been synthesized, characterized and applied as non-doped emitters in organic light-emitting devices (OLEDs). The compounds show high fluorescent quantum yields high up to 87.51 % in solid powder state as well as good thermal and film-forming properties. Crystal structures of the 2N-PI, 1N-BPI and 2N-API were determined by X-ray crystallography. Correlations between optoelectronic properties, energy levels and molecular structures of the materials were investigated. It was found that fluorescent properties of the materials were related to the dihedral angles and moiety replacement position. N-1-imidazole modification (eg: 2N-API) favours for deep-blue emission, although relatively lower quantum yield, it shows comparable device efficiency towards C-2-imidazole derivative (eg: 2N-BPI).

Introduction

Deep-blue organic light-emitting materials are important for their capability 1) of white light emission via energy-transfer to longer wavelength emitters; 2) to serve as host materials for blue phosphorescence OLED; 3) to reduce power consumption in both full-colour display and solid-state lighting.[1]

Most blue emitters reported so far are based on anthracene, fluorene, pyrene, carbazole derivatives.[1a] However, these scaffold still have many problems need to be settled, such as the easy crystallization of anthracene derivatives in the thin-film state, the fluorenone defects formation of fluorene derivatives caused by thermal or photo-oxidation, the colour purity of pyrene derivatives and the electron-transporting ability of the carbazole derivatives need to be improved.[2] In the past few years, organic emitters based on phenanthroimidazole (PI) skeleton have drawn much attention for their applications in bio-imaging,[3] sensing,[4] electrochemical luminescent cell,[5] aggregation induced emission[6] and especially organic light emitting diodes (OLED).[7-15] Phenanthroimidazole (PI) scaffold is easy for molecule modification on N-1 and C-2 position, on the other hand, the rigid skeleton as well as the bipolar property of imidazole endow it with high quantum yields, high carrier mobilities, high thermal stability, as well as good film forming ability, leading to promising applications as blue emitters in high performance OLEDs.[8-15]

In our previous work, we have obtained highly fluorescent blue emitters by attaching a thiophene ring to the C-2 position of the PI skeleton; however, the emission colour was not yet deep blue.[8a] For example, cyan and green emissions peaking at 487 nm and 521 nm were obtained in thin films of TPA-TPI and Py-TPI, respectively (See in Fig.S1). This can be attributed to two reasons: (1) the thiophene ring tends to move up the HOMO energy thus leads to narrower energy gap; (2) the thiophene ring and the imidazole ring is coplanar with small dihedral angle, leading to large emission redshifts in solid state. Bulky polyaromatic hydrocarbon groups were then introduced to reduce intermolecular interactions in solid state, although device efficiency have been improved, the colour is not yet deep-blue.[8b]

When the thiophene ring is replaced by benzene ring, the obtained dyes show deep-blue emission in thin solid film state (436 nm for TPA-BPI, 451 nm for Py-BPI, see in Fig.S1).[8c, 9] The benzene ring leads to deeper HOMO energy levels, and the larger dihedral angle between benzene ring and the imidazole ring successfully restrained intermolecular aggregation in the solid film state. Subsequently, many other efforts have been tried to develop deep-blue PI-based emitters with high device efficiency. These include construction of hybrid donor-acceptor (D-A) molecule with HLCT (hybrid local and charge transfer) excited state;[10] connecting moieties such as pyrene,[9] anthracene,[11] carbazole,[12] polyaromatic hydrocarbon groups,[13] classical AIE (aggregation induced emission) moiety of TPE[14] *etc.* to the PI skeleton via a benzene bridge; construction of *di* or *tri*-PI connected by C-2 imidazole through different position on benzene ring or naphthalene ring.[14] However, deep-blue PI derivatives with $CIE_y < 0.12$ are still rare.[8]

[a] Institute of Molecular Science, Shanxi University, Taiyuan 030006, Shanxi Province, China
[b] Department of Chemistry, Shantou University, Guangdong 515063, China. E-mail: Flu@stu.edu.cn; qxtong@stu.edu.cn

Electronic Supplementary Information (ESI) available: crystal data, CCDC 1472363-1472365. For ESI and or crystallographic data in CIF see DOI: 10.1039/c000000x/.

View Article Online DOI: 10.1039/C6RA13605B

The above strategies mainly involve modifying the molecule at the C-2 position of the PI skeleton. There are relative few attempts on N-1 modification of the PI unit, although it shows good potential for deep-blue emission.[16] In this work, we carry out systematic studies on the effects of simultaneous tuning the conjugation lengths of aromatic moieties attaching to the N-1 and the C-2 positions of the PI skeleton. Performance of eight deep-blue PI-based emitters in OLEDs were compared and correlated to their molecules structures.

The emitters were found to give deep-blue emissions with peak wavelength ranging from 395 nm to 439 nm in thin solid film state, while attaching bulky aromatic moiety such as anthracene and pyrene leads redshift of the emission wavelength (466 nm and 451 nm). The emitters show high fluorescent quantum yield as high as 87.51 % in the solid powder state.

Non-doped deep-blue OLEDs with simple three-layer structure using these emitters were observed to show deep-blue emission with CIE_y coordinate smaller than 0.12 and best efficiencies of 1.51 cd/A and 1.64 lm/W. In addition to low turn-on (i.e 2.5 ~ 4.0 V), the present devices also show stable emission colour and little efficiency roll-off at high brightness output. It is noted that the isomers with the moiety at the different position of the PI skeleton exhibit obvious different properties, for example, 2N-API shows deeper HOMO energy level (5.59 eV) and emits at shorter wavelength (399 nm) compared with 2N-BPI (439 nm) in the thin film state (HOMO: 5.27 eV). Although with much lower fluorescent quantum yield, the device efficiency of 2N-API is comparable with 2N-BPI, it might be caused by the HLCT excited state generation in the 2N-API.[10]

Experiment

General information

Nuclear magnetic resonance (NMR) spectra were recorded using CD_2Cl_2 as solvent with a Bruker AVANCE III 600 MHz spectrometer (^{1}H NMR spectra can be seen in supporting information). Mass spectra were recorded on a PE SCIEX API-MS system. Elemental analysis (C, H and N) was performed using a Vario EL III CHNS elemental analyzer. Single crystal structures were studied using X-ray diffraction with a Bruker Smart Apex CCD diffractometer (Mo Kα, λ = 0.71073 Å) using SMART [Bruker AXS, Madison, WI, USA, 1997]. Crystallographic calculations were conducted using the SHELXL-97 programs (CIFs are available in the ESI†). Absorption and photoluminescence (PL) spectra of the materials were recorded on a Perkin-Elmer Lambda 2S UV–visible spectrophotometer and a Perkin-Elmer LS50 fluorescence spectrometer, respectively. Absolute fluorescence quantum yields in solid powder state (Φ_f) were determined using an integrating sphere on an Edinburgh Instruments FLS980. Thermogravimetric (TGA) measurements were performed on a TA Instrument TGA Q50 with a heating rate of 10 °C min^{-1} under a nitrogen atmosphere. Differential scanning calorimetric (DSC) measurements were performed on a TA Instrument DSC2910. The samples were firstly heated at a rate of 10 °C min^{-1} to melt and then quenched. Glass transition temperatures (T_g) and crystallization temperatures (T_c) were recorded by heating the quenched samples at a heating rate of 10 °C min^{-1}. Ionisation potential (Ip) of the samples were measured with their thin-films on ITO glass substrates via ultra-violet photoelectron spectroscopy (UPS) in a VG ESCALAB 220i-XL surface analysis system, while the values of electron affinity (EA) were estimated by subtracting from Ip (obtained from UPS spectrum, see in supporting information) with the optical band gap (E_{gap}) determined from the onset wavelength of the absorption spectra in their solid-state films.

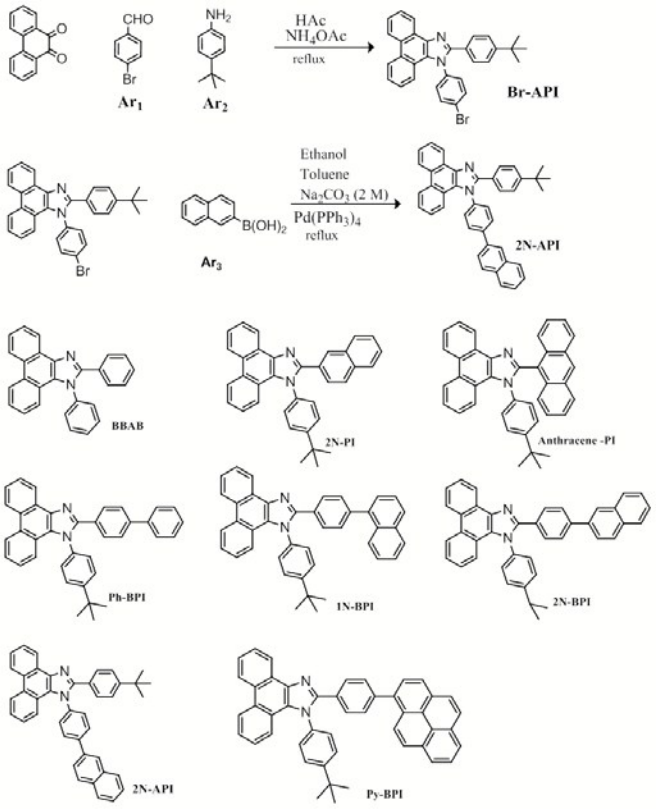

Scheme 1. Synthetic Routes and chemical structure for the Phenanthroimidazole Derivatives

OLED fabrication

Patterned indium-tin oxide (ITO) coated glass substrates with a sheet resistance of 30 Ω per square were sequentially cleaned with isopropyl alcohol, Decon 90, rinsed in de-ionized water, then dried in an oven, and finally treated in an ultraviolet-ozone chamber. The ITO substrates were then transferred into a deposition chamber with a base pressure of 10^{-6} mbar. Devices with a configuration of ITO/NPB (70 nm)/emitter (40 nm)/TPBI or BPhen (20 nm)/LiF (0.5 nm)/Mg:Ag (80 nm) were prepared by thermal vapour deposition. In the devices, NPB (4,4'-bis[N-(1-naphthyl)-N-phenyl amino] biphenyl) was used as the hole-transporting layer (HTL), BPhen (4,7-diphenyl-1,10-phenanthroline) or TPBI (1,3,5-Tris(1-phenyl-1H-benzimidazol-2-yl)benzene) were used as the electron-

transporting layer (ETL). Deposition rates for both organic and metal layers were monitored with a quartz oscillation crystal and controlled at 1–2 Å S^{-1}. A shadow mask was used to define the cathode to make four 0.1 cm^2 devices on each substrate. Electroluminescence (EL) spectra, CIE coordinates, and current density–voltage–luminance (J–V–L) characteristics of OLEDs were measured with a programmable Keithley model 237 power source and Spectra scan PR 650 photometer under ambient conditions without encapsulation.

Synthesis

All solvents and materials were used as received from commercial suppliers. Synthetic routes and the chemical structure of the synthesized compounds of the PI derivatives are outlined in Scheme 1 which were prepared according to previous literatures.

Synthesis of 1-(4-bromophenyl)-2-(4-tert-butylphenyl)-1H-phenanthro[9,10-d]imidazole (Br-API)

The product was prepared by refluxing 9,10-phenanthrenequinone (2.12 g, 10 mmol), 4-*tert*-butylbenzaldehyde (1.62 g, 10 mmol), 4-bromobenzenamine (2.06 g, 12 mmol) and ammonium acetate (9.49 g, 122.3 mmol) in glacial acetic acid (50 mL) for 24 hours under an argon atmosphere. After cooling to room temperature, a pale yellow mixture was obtained and poured into a methanol solution under stirring. The separated solid was filtered off, washed with methanol and dried to give a pale yellow solid. The solid was purified by column chromatography (petroleum ether: CH_2Cl_2, 1:1) on silica gel. A white powder was finally obtained after it was stirred in refluxing ethanol, subsequently filtered and dried in vacuum. Yield: 3.37 g (67%). ^{1}H NMR (400 MHz; CD_2Cl_2; Me_4Si) δ 1.33 (s, 9H), 7.23 (d, *J* = 8.2 Hz, 1H), 7.30−7.59 (m, 8H), 7.63−7.82 (m, 4H), 8.77 (dd, *J* = 17.3, 8.1 Hz, 3H). ^{13}C NMR (75 MHz, CD_2Cl_2) δ 31.10 (s), 34.81 (s), 72.35 (s), 120.92 (s), 122.70 (s), 123.26 (d), 123.96 (s), 124.32 (s), 125.09 (s), 125.48 (s), 125.77 (s), 126.63 (s), 127.30−128.36 (m), 128.37 (s), 129.18 (d), 131.05 (s), 133.63 (s), 137.94 (d), 138.38−138.75 (m), 151.08 (s), 152.46 (s). MS (ESI^+): m/z 505.1 (MH^+). Calcd for $C_{31}H_{25}BrN_2$: 504.12.

Synthesis of 2-(4-(tert-butyl)phenyl)-1-(4-(naphthalen-2-yl)phenyl)-1H-phenanthro[9,10-d]imidazole (2N-API)

A solution of Br-API (1.26 g, 2.5 mmol), naphthalen-2-ylboronic acid (0.65 g, 3.78 mmol), $Pd(PPh_3)_4$ (0.14 g, 0.12 mmol), and aqueous Na_2CO_3 (2 M, 9 mL) in toluene (18 mL) and ethanol (6 mL) was heated to reflux in an argon atmosphere for 24 h. The solution was cooled to room temperature and extracted with dichloromethane. The extracts were dried with anhydrous Na_2SO_4 and concentrated by rotary evaporation. The residue was purified by column chromatography (petroleum ether: CH_2Cl_2, 1:1) to obtain the pure product as white powder. Yield: 0.86 g (62%). mp: 390 °C. ^{1}H NMR (600 MHz, CD_2Cl_2) δ 8.91-8.75 (m, 3H), 8.31 (s, 1H), 8.05 (dd, *J* = 20.1, 7.5 Hz, 4H), 7.98 (s, 2H), 7.83-7.77 (m, 1H), 7.63 (ddd, *J* = 58.9, 22.5, 7.4 Hz, 8H), 7.46-7.32 (m, 4H), 1.29 (d, *J* = 63.7 Hz, 9H). ^{13}C NMR (151 MHz, CD_2Cl_2) δ 152.61 (s), 150.95 (s), 142.38 (s), 137.96 (s), 136.78 (s), 133.67 (s), 133.00 (s), 132.19 (s), 130.91 (s), 129.57 (s), 128.92 (dd, *J* = 34.3, 16.3 Hz), 128.32 (t, *J* = 17.0 Hz), 127.74 (d, *J* = 19.5 Hz), 127.20 (d, *J* = 30.8 Hz), 126.63 (s), 126.58-126.28 (m), 126.16 (d, *J* = 9.0 Hz), 125.85 (s), 125.54 (s), 125.31 (d, *J* = 11.7 Hz), 125.23-124.73 (m), 124.73-124.65 (m), 124.07 (s), 123.21 (d, *J* = 6.1 Hz), 122.66 (s), 121.13 (s), 120.98 (s), 34.57 (d, *J* = 11.4 Hz), 30.85 (d, *J* = 16.0 Hz). MS (ESI^+): m/z 553.26 (MH^+). Calcd for $C_{41}H_{32}N_2$: 552.72. Anal. Calc. for $C_{41}H_{32}N_2$: C, 89.10; H, 5.84; N, 5.07. Found: C, 89.03; H, 5.80; N, 5.01.

1,2-diphenyl-1H-phenanthro[9,10-d]imidazole (BBAB)

^{1}H NMR (600 MHz, CD_2Cl_2) δ 8.93 – 8.75 (m, 3H), 7.80 (t, *J* = 7.3 Hz, 1H), 7.68 (ddd, *J* = 31.7, 16.4, 7.5 Hz, 6H), 7.57 (dd, *J* = 9.8, 8.4 Hz, 3H), 7.35 (ddd, *J* = 22.8, 14.3, 7.5 Hz, 4H), 7.23 (d, *J* = 8.1 Hz, 1H). ^{13}C NMR (151 MHz, CD_2Cl_2) δ 130.39-130.36 (m), 130.03 (d, *J* = 41.3 Hz), 129.42 (s), 129.29-129.18 (m), 129.01 (d, *J* = 28.9 Hz), 128.13 (s), 127.35 (s), 126.37 (s), 125.64 (s), 124.98 (s), 124.05 (s), 123.18 (s), 122.63 (s), 120.93 (s). MS (ESI^+): m/z 371.0 (MH^+), Calc. For $C_{27}H_{18}N_2$: 370.15. Anal. Calc. for $C_{27}H_{18}N_2$: C, 87.54; H, 4.90; N, 7.56. Found: C, 87.49; H, 4.85; N, 7.51.

1-(4-tert-butylphenyl)-2-(naphthalen-2-yl)-1H-phenanthro[9,10-d]imidazole(2N-PI)

^{1}H NMR (600 MHz, CD_2Cl_2) δ 8.94-8.76 (m, 3H), 7.97-7.90 (m, 2H), 7.89-7.79 (m, 3H), 7.76-7.66 (m, 4H), 7.63 – 7.48 (m, 5H), 7.36 (q, *J* = 8.3 Hz, 2H), 1.50 (s, 9H). ^{13}C NMR (151 MHz, CD_2Cl_2) δ 153.64 (s), 150.60 (s), 136.09 (s), 133.07 (s), 132.80 (s), 129.40-129.32 (m), 129.32-128.21 (m), 128.21-128.11 (m), 127.60 (s), 127.56-127.14 (m), 126.83 (s), 126.65 (s), 126.35 (s), 125.56 (s), 124.93 (s), 124.02 (s), 123.20 (s), 122.54 (s), 121.09 (s), 34.96 (s), 31.14 (s). MS (ESI^+): m/z 477.2 (MH^+), Calc. For $C_{35}H_{28}N_2$: 476.23. Anal. Calc. for $C_{35}H_{28}N_2$: C, 88.20; H, 5.92; N, 5.88. Found: C, 88.15; H, 5.89; N, 5.85.

2-(anthracen-10-yl)-1-(4-tert-butylphenyl)-1H-phenanthro[9,10-d]imidazole(Anthracene-PI)

^{1}H NMR (600 MHz, CD_2Cl_2) δ 8.87 (dd, *J* = 31.5, 8.4 Hz, 3H), 8.60 (s, 1H), 8.08 (d, *J* = 8.0 Hz, 2H), 7.77 (dd, *J* = 19.9, 7.7 Hz, 4H), 7.62 (s, 1H), 7.51 (t, *J* = 7.8 Hz, 4H), 7.34 (t, *J* = 7.3 Hz, 1H), 7.27 (d, *J* = 8.0 Hz, 2H), 7.19 (dd, *J* = 20.2, 8.2 Hz, 3H), 1.20 (s, 9H). ^{13}C NMR (151 MHz, CD_2Cl_2) δ 132.18 (s), 130.89 (s), 128.47 (s), 127.05 (s), 126.68 (s), 126.43 (s), 126.17 (s), 125.73 (s), 125.38 (s), 124.06 (s), 123.23 (s), 121.14 (s), 34.54 (s), 30.78 (s). MS (ESI^+): m/z 527.5 (MH^+), Calc. for $C_{39}H_{30}N_2$: 526.24. Anal. Calc. for $C_{39}H_{30}N_2$: C, 88.94; H, 5.74; N, 5.32. Found: C, 88.87; H, 5.70; N, 5.28.

Synthesis of 2-(4-bromophenyl)-1-(4-(tert-butyl)phenyl)-1H-phenanthro[9,10-d]imidazole (Br-BPI)

Br-BPI was prepared with the similar procedure as that of Br-API. 4.03 g (79%). ^{1}H NMR (400 MHz; CD_2Cl_2; Me_4Si) δ H [ppm]: 1.47 (s, 9H), 7.16-7.83 (m, 13H), 8.76 (dd, *J* = 15.2, 8.2 Hz, 3H). ^{13}C NMR (75 MHz; CD_2Cl_2; Me_4Si) δ 31.32 (s), 35.15 (s), 121.18 (s), 122.62 (s), 123.30 (d), 124.20 (s), 125.16 (s), 125.77 (s), 126.53 (s), 127.46 (d), 128.49 (d), 129.33 (s), 130.05 (s), 130.91 (s), 131.47 (s), 135.98 (s), 137.46 (s), 149.88 (s), 153.90 (s). MS (ESI^+): m/z 505.5 (MH^+), Calc. for $C_{31}H_{25}BrN_2$: 504.12.

Synthesis of 2-([1,1'-biphenyl]-4-yl)-1-(4-(tert-butyl)phenyl)-1H-phenanthro[9,10-d]imidazole (Ph-BPI)

Ph-BPI was prepared with the similar procedure as that of 2N-API. ^{1}H NMR (400 MHz, CD_2Cl_2) δ1.49 (s, 9H), 7.26 (d, *J* = 7.4 Hz, 1H), 7.38 (t, *J* = 7.4 Hz, 1H), 7.52 (ddd, *J* = 22.0, 16.2, 8.1 Hz, 7H), 7.74 -7.62 (m, 7H), 7.78 (t, *J* = 7.4 Hz, 1H), 7.34-7.29 (m, 1H), 8.86 -8.74 (m, 3H). ^{13}C NMR (151 MHz, CD_2Cl_2) δ 153.58 (s), 150.47 (s), 141.15 (s), 140.13 (s), 136.02 (s), 129.60 (s), 129.07 (s), 128.84 (s), 128.47 (d, *J* = 8.9 Hz), 128.18 (s), 127.66 (s), 127.23 (d, *J* = 13.7 Hz), 126.91 (s), 126.64 (s), 126.32 (s), 125.52 (s), 124.87 (s), 124.00 (s), 123.18 (s), 122.52 (s), 120.99 (s), 34.94 (s), 31.14 (s). MS (ESI$^+$): m/z 503.5 (MH^+), Calc. for $C_{37}H_{30}N_2$: 502.24. Anal. Calc. for $C_{37}H_{30}N_2$: C, 88.41; H, 6.02; N, 5.57. Found: C, 88.35; H, 5.98; N, 5.53.

Synthesis of 1-(4-(tert-butyl)phenyl)-2-(4-(naphthalen-1-yl)phenyl)-1H-phenanthro[9,10-d]imidazole (1N-BPI)

^{1}H NMR (400 MHz, CD_2Cl_2) δ 1.48 (s, 9H), 7.27-7.38 (m, 2H), 7.43-7.61 (m, 9H), 7.67-7.83 (m, 6H), 7.92 (dd, *J* = 16.7, 8.1 Hz, 3H), 8.75-8.89 (m, 3H). ^{13}C NMR (151 MHz, CD_2Cl_2) δ 133.86 (s), 131.31 (s), 129.84 (s), 129.19 (s), 128.52 (s), 128.28 (s), 127.89 (s), 127.23 (s), 126.91 (s), 126.40 (s), 126.15 (s), 126.15-125.89 (m), 125.76 (d, *J* = 30.7 Hz), 125.37 (s), 124.04 (s), 123.20 (s), 121.06 (s), 34.96 (s), 31.12 (s). MS (ESI$^+$): m/z 553.7 (MH^+), Calc. for $C_{41}H_{32}N_2$: 552.26. Anal. Calc. for $C_{41}H_{32}N_2$: C, 89.10; H, 5.84; N, 5.07. Found: C, 89.04; H, 5.78; N, 5.00.

Synthesis of 1-(4-(tert-butyl)phenyl)-2-(4-(naphthalen-2-yl)phenyl)-1H-phenanthro[9,10-d]imidazole (2N-BPI)

^{1}H NMR (600 MHz, CD_2Cl_2) δ 1.51 (s, 9H), 7.28 (d, J = 7.7 Hz, 1H), 7.33 (dd, *J* = 11.1, 4.1 Hz, 1H), 7.59 – 7.52 (m, 5H), 7.76 – 7.69 (m, 5H), 7.80 (dd, J = 16.4, 8.4 Hz, 4H), 7.99 – 7.90 (m, 3H), 8.13 (s, 1H), 8.81 (dd, J = 30.4, 8.3 Hz, 2H), 8.89 (d, *J* = 7.7 Hz, 1H). ^{13}C NMR (151 MHz, CD_2Cl_2) δ 153.62 (s), 150.42 (s), 140.99 (s), 137.40 (s), 136.03 (s), 133.66 (s), 132.81 (s), 129.68 (s), 129.09 (s), 128.50 (d, *J* = 3.3 Hz), 128.20 (s), 127.57 (s), 127.26 (d, *J* = 10.9 Hz), 126.89 (s), 126.40 (s), 126.25 (d, *J* = 26.2 Hz), 125.69 (s), 125.55 (s), 125.12 (s), 124.89 (s), 124.01 (s), 123.19 (s), 122.54 (s), 121.01 (s), 34.96 (s), 31.15 (s). MS (ESI$^+$): m/z 553.6 (MH^+), Calc. for $C_{41}H_{32}N_2$: 552.26. Anal. Calc. for $C_{41}H_{32}N_2$:C, 89.10; H, 5.84; N, 5.07. Found: C, 89.04; H, 5.79; N, 5.03.

Results and discussion

X-ray Crystal Structures

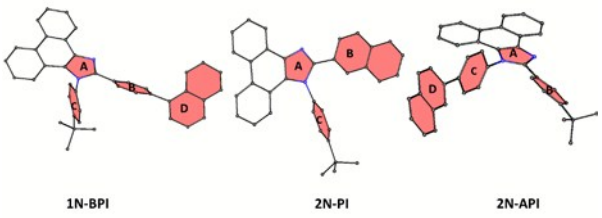

Fig.1 Molecule structures of the 1N-BPI, 2N-BPI and 2N-API.

Single crystals of 2N-PI, 1N-BPI, 2N-API were obtained by diffusing n-hexane into dichloromethane solutions of the compounds (CCDC NO. 1472363-1472365). Dihedral angle and intermolecular interaction analysis of the single crystals are shown in TableS1 and Fig.S2-S4. Fig.1 shows molecule structures of the three compounds, in which we can see that (1) N-1 moieties have large twisted dihedral angle of 64.15 °, 86.33 °, 83.64 ° towards PI skeleton for 1N-BPI, 2N-PI and 2N-API, respectively; (2) Attaching moieties to C-2 position of PI with benzene ring as linker show rather larger twisted dihedral angle (36.04 ° in 1N-BPI and 33.27 ° in 2N-API) than that of 2N-PI (1.86 °) which attached 2-naphthalene ring directly to the imidazole skeleton; (3) naphthalene ring attached to the N-1 and C-2 PI through benzene ring shows twisted angle of 53.71 ° and 36.23 ° towards the benzene ring. This indicates that 1N-BPI and 2N-API exhibit more twisted structure while attaching bulky moiety (naphthalene in this case) directly to C-2 PI leads to planar structure for 2N-PI.

The twisted structure of 1N-BPI and 2N-API can suppress intermolecular stacking effectively with π-π interaction of 4.15 ~ 6.07 Å and C-H···π interaction of 2.99 ~ 3.18 Å in solid state and thus prevent self-quenching of fluorescence, this can be seen directly in Fig.S3 and Fig.S4. As expected, the planar structure of 2N-PI shows relatively more condensed packing with stronger π-π interaction of 3.54 Å, 3.87 Å, 3.93 Å and C-H···π interaction of 2.98 Å, 3.40 Å (Fig.S2).

Thermal Properties

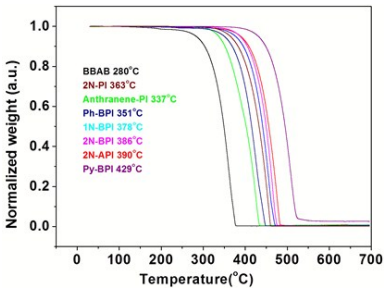

Fig.2 TGA curves of the synthesized phenanthroimidazole derivatives

Thermal properties of the eight PI derivatives were investigated with TGA (Fig.2) and DSC (Fig.3) under a nitrogen atmosphere. Key thermal data of the compounds are summarized in Table 1. All the compounds exhibited good thermal stability. Decomposition temperatures (T_d), defined as the temperature at which the material showed a 5 % weight loss, were measured to be 280, 363, 337, 351, 378, 386, 390 and 429 °C for BBAB, 2N-PI, Anthracene-PI, Ph-BPI, 1N-BPI, 2N-BPI, 2N-API and Py-BPI, respectively. DSC measurements have been performed, from 20 to 280 °C for BBAB and 1N-BPI and from 20 to 330 °C for 2N-PI, Anthracene-PI, Ph-BPI, 2N-BPI, 2N-API and Py-BPI, respectively. There appears to be a glass transition temperature (T_g) in the range of 80-137 °C for all of the materials (Fig.3). It is observed that in the second heating

View Article Online
DOI: 10.1039/C6RA13605B

Journal Name

ARTICLE

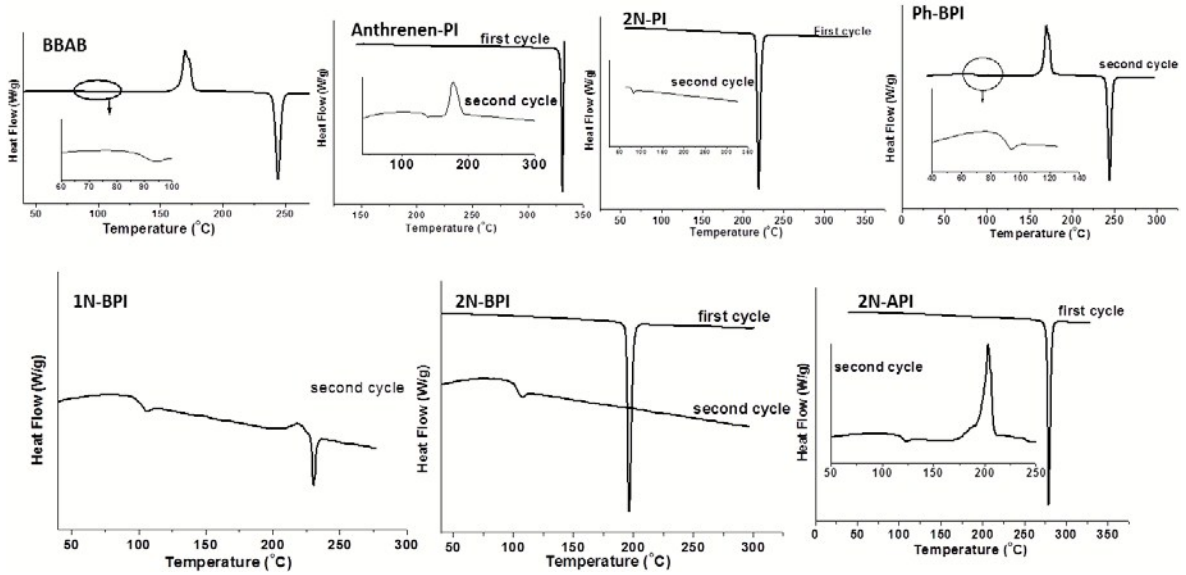

Fig.3 DSC curves of the synthesized phenanthroimidazole derivatives.

process there appears to be a crystallization temperature (T_c) of 120, 176, 169, 203 °C for BBAB, Anthracene-PI, 1N-BPI, 2N-API, respectively.

From these results we can see that: (1) T_d of BBAB (280 °C) is much lower than those of compounds with larger aromatic moieties at the N-1 and the C-2 positions, indicating the large conjugation favours the better thermal stability; (2) T_g of BBAB is higher than 2N-PI and Ph-BPI, it might due to the more relaxed packing of the two compounds in solid state; (3) the other five compounds have higher T_g above 100 °C for their larger extent of conjugation and stronger intermolecular interaction; (4) swapping of the aromatic moieties at the N-1 and the C-2 positions in 2N-API and 2N-BPI leads to considerable changes in T_d (386 °C *vs* 378 °C) and T_g (123 °C *vs* 105 °C), while attaching 1- or 2-naphthalen onto C-2-imidazole (1N-BPI, 2N-BPI) cause little change in T_g. This result suggests that it can effectively increase the thermal stability when attaching naphthalene ring via a benzene ring on N-1-imidazole rather than on C-2-imidazole; (5) Py-BPI exhibits the best thermal properties among the eight compounds, owing to the rigidity of the pyrene moiety.

Optical properties

Fig.4 depicts absorption and PL spectra of the eight materials measured in both dichloromethane solutions and thin solid films on quartz substrates. Intensive blue emissions peaked at wavelengths ranging from 395 to 466 nm were observed. Key optical parameters are summarized in Table 1. As is shown in Fig.4a,c that in CH_2Cl_2 solutions and solid film state, all compounds show similar absorption peaks at *ca.* 260 nm, which may originate from their common benzene ring. In addition, the absorption band between 300 nm to 400 nm is assigned to the π–π* electronic transition in the phenanthroimidazole. Deep-blue emissions were observed for BBAB (388 nm), 2N-PI (399 nm) and 2N-API (394 nm) owing to their smaller conjugations. Blue emissions peaking at wavelength ranging from 410 to 439 nm were observed for compounds of Ph-BPI (410 nm), 1N-BPI (415 nm), 2N-BPI (419 nm), Py-BPI (439 nm). Of which, Py-BPI has larger conjugation with bulk pyrene in the skeleton, resulting in red shift in emission spectra with more narrow energy gap (2.63 eV), which can be measured by the onset wavelength of the absorption in the film state.[8a] (1) From solution state (Fig. 4b) to thin film (Fig. 4d), relatively small redshifts were observed in the PL peaks of BBAB (7 nm), Anthracene-PI (5 nm), Ph-BPI (15 nm), 1N-BPI (7 nm), 2N-BPI (20 nm), 2N-API (5 nm), Py-BPI (12 nm). A much larger redshift of 31 nm was observed in 2N-PI probably due to the planarity of its structure with strong intermolecular interaction of 3.54 Å when attaching 2-naphtalene directly to C-2-imidazole with a dihedral angle degree of 1.86 ° only (Fig.1, Table S1 and Fig.S2); (2) 2N-API shows deep-blue emission located at 399 nm in thin film state while its isomer of 2N-BPI emits at 439 nm, 1N-BPI is similar to 2N-BPI emitting at 422 nm.[8a] It can be correlated to the dihedral parameters of the crystal structure as shown in Table S1. The "C-ring" towards "A-ring" in 2N-API is highly twisted with a dihedral angle of 83.64 °, rather highly than

View Article Online
DOI: 10.1039/C6RA13605B

that in 1N-BPI (64.15 °), on other hand, the π···π interaction of phenanthro ring and the imidazole ring in 2N-API is larger (5.89 Å) than that of 1N-BPI between imidazole ring and imidazole ring (4.65 Å) resulting in deeper blue emission. This suggests that attaching bulky moiety through benzene ring to N-1 position rather than to C-2 position of PI favours for deep blue emission by successfully restrained intermolecular aggregation.

All of the eight compounds show strong emission in solid state with rather high quantum yield from 58.21 % to 87.51 % (Table1). Among these compounds, 2N-PI and 2N-API show relatively low quantum yield of 69.51 % and 58.21 % respectively, this might be due to the self-quenching caused by much planar structure of 2N-PI and low conjugation of much twisted structure of 2N-API. However, compounds with C-2 modification PI through benzene ring show relatively high quantum yields up to 87.51 % for 2N-BPI. The results indicate that compounds of N-1 PI show deeper blue emission however relatively low quantum yield, while C-2 PI connected through benzene ring show high luminescent efficiency with emission red-shifted to longer wavelength.

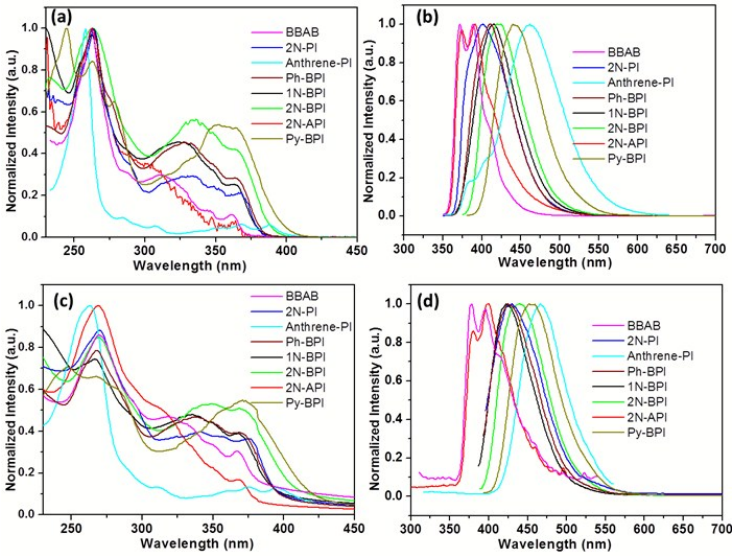

Fig.4 Absorption and PL spectra of the phenanthroimidazole derivatives in CH_2Cl_2 solutions (a, b) and solid film state (c, d).

Table.1 Photophysical properties and energy levels of the eight phenanthroimidazole derivatives

Compounds	$T_m/T_g/T_d$ (°C)	$^a\Phi_f$	Abs_{max}(nm) [b]/[c]	PL_{max}(nm) [b]/[c]	^{c}HOMO (eV)	^{c}LUMO (eV)	$^c Abs_{onset}$ (nm)	Energy Gap (eV)
BBAB	205/95,120*/280	42.79 %	361/368	371,388/377,395	5.64	2.54	400	3.10
2N-PI	220/80/363	69.51 %	366/377	399/430	5.33	2.27	405	3.06
Anthracene-PI	325/125,176*/337	82.36 %	388/395	461/466	5.51	2.43	403	3.08
Ph-BPI	244/93,169*/351	65.30 %	364/372	410/ 425	5.41	2.39	411	3.02
1N-BPI	230/102/378	73.58 %	364/368	415/422	5.41	2.38	409	3.03
2N-BPI	196/105/386	87.51 %	365/369	419/439	5.27	2.37	427	2.90
2N-API	279/123,203*/390	58.21 %	363/368	371, 394/380,399	5.59	2.46	396	3.13
Py-BPI	300/137/429	80.46 %	362/371	439/451	5.35	2.68	464	2.67

[a] absolute quantum yield obtained from solid powder by integrating sphere. [b] obtained from the dilute solution in dichloromethane solvent. [c] obtained from the thin film state. * crystal temperature.

View Article Online
DOI: 10.1039/C6RA13605B

Journal Name

ARTICLE

Table.2 Device performance parameters obtained using the phenanthroimidazole derivatives as emitter.

Emitters	[c]V_{onset} (V)	V at 20 mA/cm^2/(V)	[d]PL (nm)	EL (nm)	CE_{max} (cd/A)	PE_{max} (lm/w)	EQE_{max} (%)	CIE(x, y)
BBAB[a]	3.9	5.7	395	448	1.51	1.02	1.53	(0.15, 0.12)
2N-PI[a]	2.8	4.3	430	448	0.89	0.78	0.95	(0.15, 0.11)
Anthracene-PI[a]	3.2	5.4	467	472	1.33	0.97	0.80	(0.16, 0.24)
Ph-BPI[a]	3.0	4.0	425	448	0.62	0.55	0.68	(0.15, 0.10)
1N-BPI[a]	3.2	4.3	422	448	0.53	0.55	0.60	(0.14, 0.10)
2N-BPI[a]	3.0	4.4	439	448	1.37	1.44	1.61	(0.14, 0.11)
2N-API[a]	3.4	4.9	399	448	1.2	1.07	1.47	(0.15, 0.11)
Py-BPI[a]	3.0	5.0	451	468	2.96	2	2.0	(0.15, 0.19)
Ph-BPI[b]	3.3	4.7	425	448	0.60	0.57	0.67	(0.14, 0.11)
1N-BPI[b]	4.0	6.7	422	448	0.71	0.45	0.76	(0.14, 0.10)
2N-BPI[b]	3.0	4.5	439	448	1.56	1.64	1.84	(0.14, 0.11)
Py-BPI[b]	2.5	4.0	451	468	3.27	3.17	2.07	(0.15, 0.18)

[a] device fabrication using TPBI as electron transporting layer [b] device fabrication using BPhen as electron transporting layer. [c] obtained at luminescent of 1 cd/m^2. [d] obtained in solid film state.

Electroluminescence (EL) performance

To investigate EL properties of the synthesized PI derivatives, devices with a simple three layer configuration structure of ITO/ NPB (60 nm) / one of emitters (40 nm) / TPBI or BPhen (20 nm) / LiF(0.5 nm) / Mg:Ag (100 nm) were fabricated. Energy level diagrams of the devices are shown in Fig.5. Fig.6-7,10a show device performance using TPBI while in Fig.8,9,10b using BPhen as electron transporting layer. Key device performance parameters are summarized in Table 2. All the fabricated devices emit brightly ranging from deep blue to cyan when positive bias was applied to the ITO.

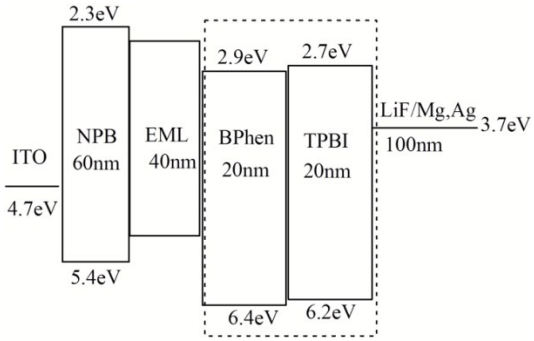

Fig.5 Device structure and energy diagram based on the phenanthroimidazole derivatives.

Fig.6a depicts normalized EL spectra of the eight devices using TPBI as the electron transporting layer. Peak wavelengths of the EL spectra for the devices using the synthesized PI derivatives as the emitting layer (EML) are 448 nm except for Anthracene-PI and Py-BPI are 472 nm and 468 nm, respectively. The EL spectra of the devices are almost the same as the corresponding PL spectra of solid films of the 2N-PI, Anthracene-PI, Ph-BPI, 1N-BPI, 2N-BPI, Py-BPI. This suggests that the EL is indeed derived from the emitters. It is noted that there are about 50 nm redshift of the EL with respect to the film PL for both BBAB and 2N-API. The inset picture of Fig.6a depicts the emission colour are deep blue corresponding to CIE coordinates of (0.15, 0.12), (0.15, 0.11), (0.15, 0.10), (0.14, 0.10), (0.14, 0.11), (0.15, 0.10) for BBAB, 2N-PI, Ph-BPI, 1N-BPI, 2N-BPI, 2N-API, blue emission colour of (0.15, 0.18) for Py-BPI and cyan emission colour of (0.16, 0.24) for Anthracene-PI.

From the above results we can see that by attaching bulky pyrene to C-2 position through benzene ring, the obtained Py-BPI based device show blue electroluminescent peaks at 468 nm with corresponding CIE coordination of (0.15, 0.19), while Anthracene-PI based device shows cyan emission with CIE coordinate of (0.16, 0.24). Attaching moiety directly on the C-2 position would cause obvious redshift of the emission from deep blue to cyan (BBAB, 2N-PI, Anthracene-PI). This suggests attaching moiety through benzene ring other than directly to C-2 PI would prevent the red-shift of the

blue emission.

Fig.6b shows J-V-L characteristics of the eight devices. The devices show maximum brightness of 5035, 4837, 4919, 3430, 2237, 4480, 3346, 7849 cd/m^2 with a voltage lower than 10 V for BBAB, 2N-PI, Anthracene-PI, Ph-BPI, 1N-BPI, 2N-BPI, 2N-API, Py-BPI as emitters respectively. Attaching of 2-naphthalene through benzene ring to PI at N-1 PI leads a deeper HOMO energy level for 2N-API (5.59 eV) than that at C-2 PI for 2N-BPI (5.27 eV). And the deeper HOMO energy of 2N-API is not beneficial for hole injection from the adjacent hole transporting layer. Thus, although 2N-API and 2N-BPI are isomers, they are much different in device performance, for example, 2N-BPI needs lower turn-on voltage of 3.0 V and operation voltage of 4.4 V (at current density of 20 mA/cm^2) with the maximum luminescent of 4480 cd/m^2, which is better than that of 2N-API for 3.4 V, 4.9 V, 3346 cd/m^2, accordingly. Although much deeper HOMO energy and lower fluorescent quantum yield, the maximum device efficiency of 2N-API (1.2 cd/A, 1.07 lm/W) is comparable with that of 2N-BPI (1.37 cd/A, 1.44 lm/W), which might be caused by the HLCT excited state generation in the 2N-API.[10]

By attaching 1-naphthalene and 2-naphthalene through benzene ring to C-2 PI, we get 1N-BPI and 2N-BPI, respectively. It shows deeper HOMO energy of 5.41 eV for 1N-BPI than 2N-BPI (5.27 eV), which might be caused by the more conjugation extent deriving from the different dihedron angel degrees between the benzene ring and the naphthalene ring.[8a] Thus, 1N-BPI based device needs higher turn-on voltage of 3.2 V and much lower device efficiency of (0.53 cd/A, 0.55 lm/W) with the maximum luminescent of 2237 cd/m^2.

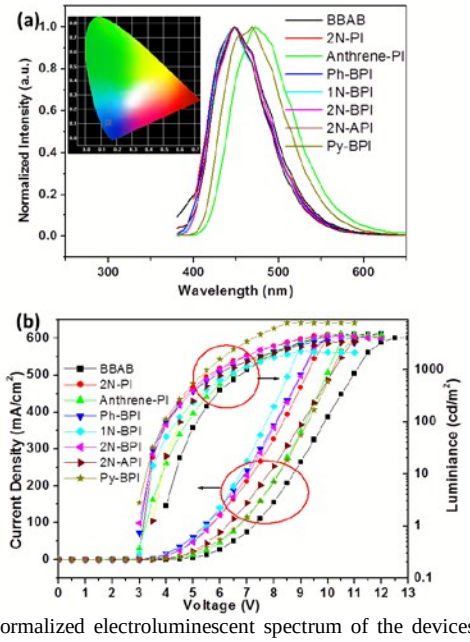

Fig.6 (a) Normalized electroluminescent spectrum of the devices based on the emitters; (b) Current density–voltage and luminance–voltage characteristics of the OLEDs based on the phenanthroimidazole derivatives with TPBI as the electron transporting layer.

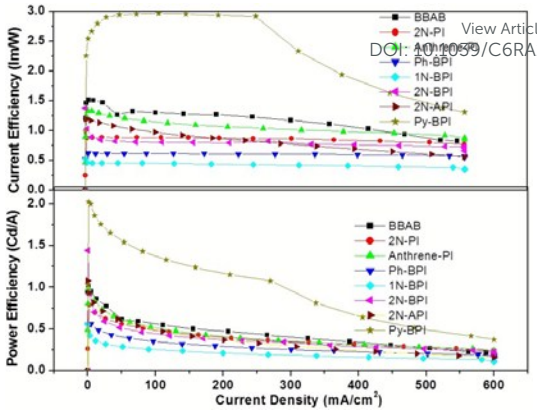

Fig.7 Current efficiencies and power efficiencies of the devices based on the phenanthroimidazole derivatives with TPBI as the electron transporting layer.

Among all of the devices, the device based on Py-BPI with CIE coordinates (0.15, 0.18) show high current efficiency (CE) and power efficiency (PE) of 2.96 cd/A and 2.0 lm/W, respectively, however the device emission is not deep blue emissions as other emitters with CIEy < 0.12. The maximum efficiencies of the other deep blue OLEDs are 1.51 cd/A (1.02 lm/W), 0.89 cd/A (0.78 lm/W), 1.33 cd/A (0.97 lm/W), 0.62 cd/A (0.55 lm/W), 0.53 cd/A (0.55 lm/W), 1.37 cd/A (1.44 lm/W), 1.2 cd/A (1.07 lm/W) respectively for BBAB, 2N-PI, Anthracene-PI, Ph-BPI, 1N-BPI, 2N-BPI, 2N-API as emitters (Table.2). The Current and power efficiencies of the devices with respect to different current density are shown in Fig.7. As is shown in Fig.7a, for all of the devices, the current efficiencies show little decrease with the increase of the current density. And for the devices with 2N-PI, Anthracene-PI, Ph-BPI and 1N-BPI, the power efficiency decreases in mild, while for the devices with BBAB and 2N-BPI show large decreases at the start then mild as current density increases (Fig.7b).

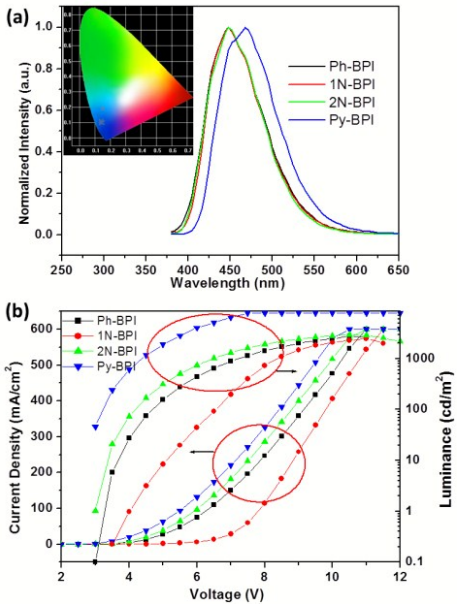

Fig.8 (a) Normalized electroluminescent spectrum of the devices based on the emitters; (b) Current density–voltage and luminance–voltage characteristics of the OLEDs based on the phenanthroimidazole derivatives with BPhen as the electron transporting layer.

By attaching moieties of benzene, 1-naphtalnene, 2-naphthalene, pyrene with different conjugation to C-2-imidazole through benzene ring we get Ph-BPI, 1N-BPI, 2N-BPI, Py-BPI. Fig.8 depicts normalized EL spectra and J-V-L characteristics of the four devices using BPhen instead of TPBI as the electron transporting layer based on these emitters. Peak wavelengths of the EL spectra for the devices are 448 nm except for Py-BPI is 468 nm. The EL spectra of the devices are almost the same as the corresponding PL spectra of solid films of the four emitters, suggesting that the EL is indeed derived from the emitters. The inset picture of Fig.8a depicts the emission colour are deep blue corresponding to CIE coordinates of (0.14, 0.11), (0.14, 0.10), (0.14, 0.11) for Ph-BPI, 1N-BPI, 2N-BPI, blue emission colour of (0.15, 0.18) for Py-BPI. Fig.8b shows J-V-L characteristics of the four devices. The devices based on Ph-BPI, 1N-BPI, 2N-BPI, Py-BPI show maximum brightness of 2431, 2786, 3017, 7771 cd/m^2 at a voltage of lower than 10 V, with turn-on voltage is 3.3, 4.0, 3.0 and 2.5 V, respectively. Fig.9 depicts the maximum device efficiency of 0.60 cd/A (0.57 lm/W), 0.71 cd/A (0.45 lm/W), 1.56 cd/A (1.64 lm/W) 3.27 cd/A (3.17 lm/W). The device efficiency decreases in mild as current density increasing, except for 2N-BPI that it has a sharp decrease at the start. Py-BPI shows the best device efficiency, however, the luminescent colour is not deep blue as that of 2N-BPI. From the result we can also see that although better device efficiency achieved using BPhen as the electron transporting layer, the turn-on voltage as well as the maxiumum luminescent is not so good as the device based on TPBI as the electron transporting layer.

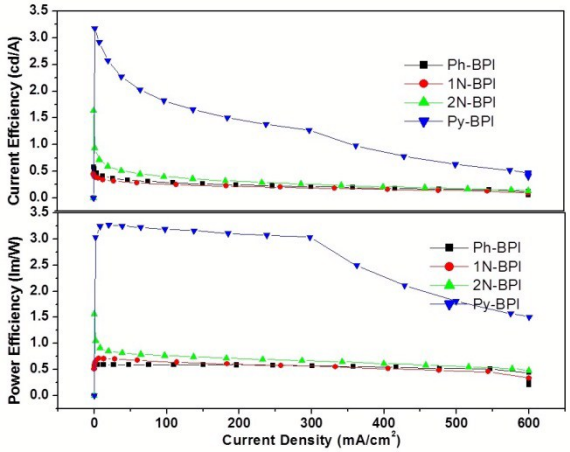

Fig.9 Current efficiencies and power efficiencies of the devices based on the phenanthroimidazole derivatives with BPhen as the electron transporting layer.

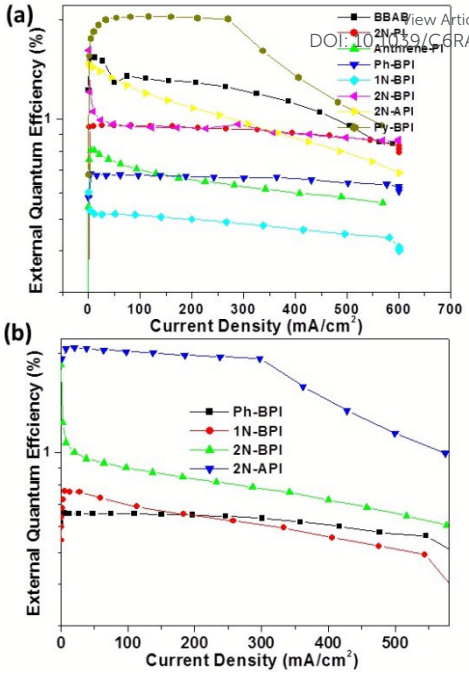

Fig.10 External quantum efficiency of the devices based on TPBI (a) or BPhen (b) as electron transporting layer.

As can be seen clearly in Fig.10 that, except for devices based on Py-BPI, the external quantum efficiency of the devices based on both TPBI and BPhen as electron transporting layer show little roll-off as current density increasing high up to 600 mA/cm^2, indicating the stability of the emitters and balanced hole/electron injection and transporting.

The devices based on these reported emitters show relatively lower efficiency but the emission colour can be successfully tuned from green to deep blue with respect to those emitters with thiophene ring attached to C-2 position of PI, suggesting the balance between the emission colour and efficiency should be considered in the molecular design.

Conclusions

Several deep blue emitters based on phenanthroimidazole derivatives have been designed and synthesized as emitters for OLED. The devices show deep blue emission with CIE < 0.12 as well as good stability with little efficiency roll-off. Among the synthesized emitters, we found that 2N-BPI and 2N-API showed relatively better performance with high device efficiency and good color purity.

The molecule structures were tuned through N-1 and C-2 position of PI modification. From single crystal structure analysis, it is found that the modification position and dihedral angle are important factors for deep blue emission and efficient luminescent. Deep blue emission can be obtained attaching aromatic moieties through benzene ring (eg: 2N-BPI) other than attaching bulky moieties directly to the C-2 position of PI (eg: 2N-PI, Anthracene-PI). Attaching aromatic moiety on N-1 position (eg: 2N-API) is effective for deep blue emission but relatively lower fluorescent

quantum yield towards emitters with C-2 position modification (eg: 2N-BPI), however, it can achieve comparable device efficiency owing to HLCT excited state generation.

Acknowledgements

This work was financially supported by the National Natural Science Foundation of China (Project No. 51273108), the National Basic Research Program of China (973 Program No. 2013CB834803) and Natural Science Foundation of Shanxi Province (206626901001), Technological Innovation Scientific and Technological Innovation Programs of Higher Education Institutions in Shanxi (206548901022), Scientific Research Start-up Funds of Shanxi University (020354010, 231545003).

References

1. (a) X. Yang, X. Xu and G. Zhou, *J. Mater. Chem. C*, **2015**, *3*, 913; (b) X. Yang, G. Zhou and W. Y. Wong, *Chem. Soc. Rev.*, **2015**, *44*, 8484; (c) M. Zhu and C. Yang, *Chem. Soc. Rev.*, **2013**, 42, 4963.
2. C. Adachi, T. Tsutsui, S. Saito, *Appl. Phys. Lett*., **1990**, *56*, 799; K. Danel, T. H. Huang, J. T. Lin, Y. T. Tao, C. H. Chuen, *Chem. Mater*., **2002**, *14*, 3860; E. J. W. List, R. Guentner, P. S. Freitas, U. Scherf, *Adv. Mater*., **2002**, *14*, 374; V. R. Nikitenko, J. M. Lupton, *J. Appl. Phys*., **2003**, *93*, 5973; J. K. Salunke, P. Sonar, F. L. Wong, V. A. L. Roy, C. S. Lee and P. P. Wadgaonkar, *Phys. Chem. Chem. Phys*., **2014**, *16*, 23320.
3. C. Jin, J. Liu, Y. Chen, G. Li, R. Guan, P. Zhang, L. Ji and H. Chao, *Dalton Trans*., **2015**, *44*, 7538.
4. (a) L. Zheng and R. Hua, J. Org. Chem. 2014, 79, 3930; (b) L. K. Zhang, Q. X. Tong and L. J. Shi, *Dalton Trans*., **2013**, *42*, 8567; (c) K. C. Song, H. Kim, K. M. Lee, Y. S. Lee, Y. Do, M. H. Lee, *Sensors and Actuators B*, **2013**, *176*, 850.
5. M. S. Subeesh, K. Shanmugasundaram, C. D. Sunesh, Y. S. Won and Y. Choe, *J. Mater. Chem. C*, **2015**, *3*, 4683.
6. (a) R. Misra, T. Jadhav, B. Dhokale and S. M. Mobin, *Chem. Commun.*, **2014**, *50*, 9076; (b) Y. Zhang, J. H. Wang, J. Zheng and D. Li, *Chem. Commun.*, **2015**, *51*, 6350.
7. (a) B. Liu, J. Zhao, C. Luo, F. Lu, S. Tao and Q. X. Tong, J. *Mater. Chem. C*, **2016**, *4*, 2003; (b) D. Liu, M. Du, D. Chen, K. Ye, Z. Zhang, Y. Liu and Y. Wang, *J. Mater. Chem. C*, 2015, *4*, 4394; (c) H. Huang, Y. Wang, B. Wang, S. Zhuang, B. Pan,X. Yang, L. Wang and C. Yang, *J. Mater. Chem. C*, **2013**, *1*, 5899; (d) Y. Yuan, D. Li, X. Zhang, X. Zhao, Y. Liu, J. Zhang and Y. Wang, *New J. Chem.*, **2011**, *35*, 1534; (e) W. C. Chen, C. S. Lee and Q. X. Tong, *J. Mater. Chem. C*, **2015**, *3*, 10957.
8. (a) Y. Zhang, S. L. Lai, Q. X. Tong, M. Y. Chan, T. W. Ng, Z. C. Wen, G. Q. Zhang, S. T. Lee, H. L. Kwonge and C. S. Lee, *J. Mater. Chem.*, **2011**, *21*, 8206; (b) Y. Yuan, J. X. Chen, W. C. Chen, S. F. Ni, H. X. Wei, J. Ye, F. L. Wong, Z. W. Zhou, Q. X. Tong, C. S. Lee, *Org. Electron.*, **2015**, *18*, 61; (c) Y. Zhang, Shiu-Lun Lai, Q. X. Tong, M. F. Lo, T. W. Ng, M. Y. Chan, Z. C. Wen, J. He, K. S. Jeff, X. L. Tang, W. M. Liu, C. C. Ko, P. F. Wang, and C. S. Lee, *Chem. Mater.*, **2012**, *24*, 61; (d) W. C. Chen, Q. X. Tong, and C. S. Lee, *Sci. Adv. Mater.*, **2015**, *7*, 2193.
9. Y. Zhang, T. W. Ng , F. Lu, Q. X. Tong, S. L. Lai, M. Y. Chan, H. L. Kwong, C. S. Lee, Dyes Pigments, **2013**, *98*, 190.
10. (a) X. Tang, Q. Bai, Q. Peng, Y. Gao, J. Li, Y. Liu, L. Yao, P. Lu, B. Yang, and Y. Ma, *Chem. Mater.*, **2015**, *27*, 7050; (b) X. Ouyang, X. Zhang, Z. Ge, Dyes Pigments, **2014**, *103*, 39; (c) M. Chen, Y. Yuan, J. Zheng, W. C. Chen, L. J. Shi, Z. L. Zhu, F. Lu, Q. X. Tong, Q. D. Yang, J. Ye, M. Y. Chan, and C. S. Lee, *Adv. Optical Mater.*, **2015**, *3*, 1215.
11. (a) G. Mu, S. Zhuang, W. Zhang, Y. Wang, B. Wang, L. Wang, X. Zhu, *Org. Electron.*, **2015**, *21*, 9; (b) S. Zhuang, R. Shangguan, J. Jin, G. Tu, L. Wang, J. Chen, D. Ma, X. Zhu, *Org. Electron*., **2012**, *13*, 3050.
12. (a) Z. Gao, Z. Wang, T. Shan, Y. Liu, F. Shen, Y. Pan, H. Zhang, X. He, P. Lu, B. Yang, Y. Ma, Org. Electro., **2014**, *15*, 2667; (b) S. Fan, J. You, Y. Miao, H. Wang, Q. Bai, X. Liu, X. Li, S. Wang, Dyes Pigments, **2016**, *129*, 34; (c) J. Peng, K. Ye, G. Zhang, Y. Zhan, J. Jia, P. Xue, R. Lu, *Synth. Met.*, **2014**, *193*, 94.
13. Y. Yuan, J. X. Chen, F. Lu, Q. X. Tong, Q. D. Yang, H. W. Mo, T. W. Ng, F. L. Wong, Z. Q. Guo, J. Ye, Z. Chen, X. H. Zhang and C. S. Lee, *Chem. Mater*., **2013**, *25*, 4957.
14. W. Qin, Z. Yang, Y. Jiang, J. W. Y. Lam, G. Liang, H. S. Kwok and B. Z. Tang, *Chem. Mater.*, **2015**, *27*, 3892.
15. (a) Z. Wang, X. Li, K. Xue, H. Li, X. Zhang, Y. Liu, Z. Yu, P. Lu and P. Chen, *J. Mater. Chem. C*, **2016**, *4*, 1886; (b) H. Liu, Q. Bai, L. Yao, H. Zhang, H. Xu, S. Zhang, W. Li, Y. Gao, J. Li, P. Lu, H. Wang, B. Yang, and Y. Ma, *Chem. Sci.*, **2015**, *6*, 3797; (c) Z. Wang, Y. Feng, H. Li, Z. Gao, X. Zhang, P. Lu, P. Chen, Y. Ma and S. Liu, *Phys.Chem.Chem.Phys*., **2014**, *16*, 10837; (d) W. C. Chen, Y. Yuan, G. F. Wu, H. X. Wei, J. Ye, M. Chen, F. Lu, Q. X. Tong, F. L. Wong, C. S. Lee, *Org. Electron.*, **2015**, *17*, 159; (e) W. C. Chen, G. F. Wu, Y. Yuan, H. X. Wei, F. L. Wong, Q. X. Tong and C. S. Lee, *RSC Adv.*, **2015**, *5*, 18067.
16. (a) Z. Wang, X. Song, H. Li, Y. Feng, and P. Lu, *Chem. J. Chin. Univ.*, **2014**, *35*, 505; (b) Z. M. Wang, X. H. Song, Z. Gao, D. W. Yu, X. J. Zhang, P. Lu, F. Z. Shen and Y. G. Ma, *RSC Adv.*, **2012**, *2*, 9635; (c) Z. Wang, Y. Feng, S. Zhang, Y. Gao, Z. Gao, Y. Chen, X. Zhang, P. Lu, B. Yang, P. Chen, Y. Ma and S. Liu, *Phys.Chem.Chem.Phys.*, **2014**, *16*, 20772; (d) S. Zhuang, R. Shangguan, H. Huang, G. Tu, L. Wang, X. Zhu, Dyes Pigments, **2014**, *101*, 93.

View Article Online
DOI: 10.1039/C6RA13605B

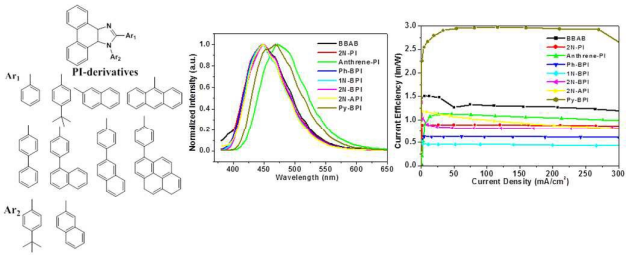

We synthesized eight phenanthroimidazole derivatives as blue emitters for OLED application and investigated relationship between the molecule structure and optoelectronic properties.